MATHEMATICS AND COMPUTATIONAL SCIENCES

Vol 2(1), 2021, pp:17-41
DOI:10.30511/mcs.2021.137964.1009
ISSN:2717-2708
http://mcs.qut.ac.ir/

QOM UNIVERSITY OF TECHNOLOGY

Seismic bearing capacity of strip footings adjacent to slopes using pseudo dynamic approach

A. Ramazan Borujerdi [1], M. Jiryaei Sharahi [2]

Abstract: Determining of the seismic bearing capacity has a great importance for foundations located near sloping ground in geotechnical earthquake engineering. In this paper a new formulation based on the pseudo-dynamic method is presented to calculate the seismic bearing capacity of strip foundations resting on C-φ soil which are adjacent to slope using limit equilibrium method. The seismic bearing capacity coefficient $N_{\gamma e}$ for the simultaneous resistance of surcharge, unit weight and cohesion is calculated considering two-sided composite rupture surface which is the combination of a logarithmic spiral and planar surfaces. This failure mechanism comprises of two slip surfaces which are assumed that a realistic failure surface occurs on the side of slope and the resistance mobilization is taken into account on the side without slope. Using the presented approach a parametric study is conducted to study the effect of various parameters such as soil cohesion, soil friction angle, slope angle, horizontal, and vertical seismic coefficients. Results show the bearing capacity coefficient increases by approximately 176 and 264% when β increases from 10 to 20° and from 20 to 30°, respectively. The results of this study are compared with the few pseudo-static results available in the literature. Present procedure give lower amount of bearing capacity of strip footings in comparison with the results of pseudo-static analysis.

Keywords: Seismic bearing capacity; Slopes; Foundations; Limit equilibrium method; Pseudo-dynamic; C-φ soil.
2020 Mathematics Subject Classification: 65M30
Receive: 10 October 2020**, Accepted:** 15 January 2020

1 Introduction

Some structures such as buildings, highways bridges and walls are often forced to be built on or adjacent to slope, particularly in region with mountainous terrains. During an earthquake phenomenon, the bearing

[1] Department of Civil Engineering, Qom University of Technology, Qom, Iran.
[2]Corresponding Author: Department of Civil Engineering, Qom University of Technology, Qom, Iran, jiryaei@qut.ac.ir

capacity of foundation is placed on sloping ground is lower than that of foundations placed on level ground. Therefore, in seismically active areas, computation of seismic bearing capacity of foundations adjacent to slope is an important issue in geotechnical engineering. Various techniques such as upper bound and lower bound limit analysis, limit equilibrium method, stress characteristics are available to calculate seismic bearing capacity of foundations. Considering pseudo-static approach, many investigators have studied several methods to determine bearing capacity of shallow foundations placed on level ground under seismic forces [2, 5, 14, 15, 16]. But a few researchers have studied the problem of bearing capacity of shallow foundations placed along a slope [4, 9, 10] or near sloping ground [1, 7, 13]. Choudhury and Subba Rao (2006) [4] and Kumar and Kumar (2003) [10] proposed the bearing capacity factors for the embedded shallow strip footings on sloping ground using limit equilibrium analysis. Kumar and Ghosh (2006) [9]used the upper bound method of limit analysis to compute the bearing capacity factors for footing embedded on sloping ground. Sarma and Chen (1995) [13] obtained seismic bearing capacity of strip footings placed near slopes by using limit equilibrium analysis. Askari and Farzaneh (2003) [1] and Ghosh and Kumar (2005) [7] determined bearing capacity factors by the use of the upper-bound limit analysis technique for strip footings adjacent to slopes. The above studies concentrated on pseudo-static analysis. It is recognised that pseudo-static loads does not take into account the time-dependent effect , oscillatory nature or phase difference of earthquake loads. To rectify these limitations of pseudo-static approach, Steedman and Zeng (1990) [17] introduced the pseudo-dynamic method considering the effect of the phase and amplitude variations of earthquake accelerations with depth, velocity of seismic waves and the period of lateral shaking to estimate the seismic earth pressure behind a retaining wall under the active failure mode. To determine seismic earth pressure behind a vertical retaining wall Choudhury and Nimbalkar (2005) [3] developed the pseudo-dynamic approach incorporating the effect of the nature of earthquake loading parameters such as time, phase difference and the effect of both shear and primary waves as well as the amplification of excitation during the earthquake. Recently, Ghosh (2008) [6] and Saha and Ghosh (2014) [11] proposed pseudo-dynamic analysis to computing seismic bearing capacity of strip footings using the Coulomb failure mechanism based on the upper-bound limit analysis method and limit equilibrium method, respectively. Under the static condition, Saran et al. (1989) [12] applied both limit equilibrium and limit analysis methods to

obtain bearing capacity for footings near slopes. However, the problem of pseudo-dynamic approach for computing the seismic bearing capacity of strip footings near slope has not been explored in previous studies. Therefore it is necessary to evaluate a seismic bearing capacity of shallow strip footings constructed adjacent to slopes considering dynamic nature of earthquake loading.

In the current study, limit equilibrium method in association with composite rupture surface similar to that discussed in Saran et al (1989) [12] is considered to develop a new formulation for calculating the seismic bearing capacity coefficient ($N_{\gamma e}$) for shallow foundations resting on C-φ soil which are adjacent to slopes using pseudo-dynamic method. In addition to the horizontal and vertical acceleration coefficients of the earthquake, the phase difference and the oscillating nature of the earthquake acceleration, and also the velocity of propagation of compressive and shear waves are considered to estimate the seismic bearing capacity of foundation adjacent slopes. Appling the presented approach a parametric study is conducted to investigate the effect of different parameters such as soil friction angle (φ), slope angle (β), cohesion factor ($2C/\gamma/b$), depth factor (D_f/b), distance of footing from the slope edge factor (D_e/b), both horizontal and vertical seismic acceleration coefficients (K_h/K_v) and time and phase difference in both the shear wave and primary wave velocities propagating through the soil on the pseudo-dynamic bearing capacity coefficient ($N_{\gamma e}$).

2 Generalized formulation

It is intended to compute pseudo-dynamic bearing capacity coefficient ($N_{\gamma e}$) attributed to component of unit weight (γ) for strip footing on slope resting on C-φ soil using limit equilibrium method. The homogeneous soil mass is assumed to be ideally plastic and Mohr-Coulomb's yield criterion is valid. The notation used in this paper is summarized in Table 1.

Fig. 1 shows a composite failure mechanism of a rough strip footing placed on a slope. In this case, a realistic rupture plane is assumed to occur along the surface ANKG. The downslope zone BNKG is larger than the zone ANDE rising to the horizontal ground surface. This means that the elastic wedge ABN is non-symmetric.

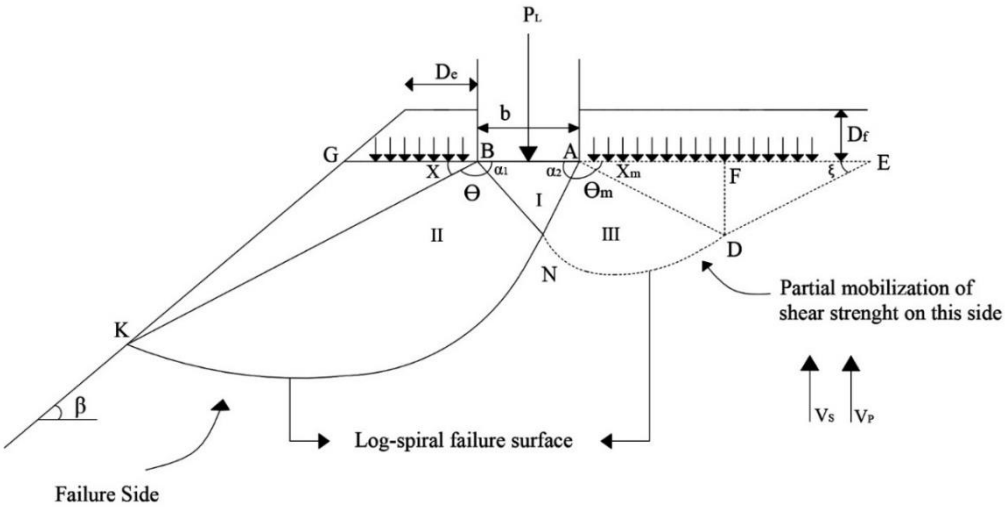

Figure 1: the failure mechanism used in the present analysis

Let α_1 and α_2 denote the angles of elastic wedge, respectively,./trf, and

$$\alpha_1 + \alpha_2 = \frac{\pi}{2} + \varphi \tag{2-1}$$

Wedge BNKG which is the combination of radial shear zone BNK and Rankine passive zone BGK bounded by a logarithmic spiral NK. The equation of the spiral curve NK can be described as follows:

$$BK = r_0 e^{\theta \, tan\varphi} \tag{2-2}$$

Where,

$$r_0 = BN = \frac{b \sin \alpha_2}{sin(\alpha_1 + \alpha_2)} \tag{2-3}$$

The wedge ANDE, shown as dotted lines in Fig.1, on the side of level ground, is partially mobilized. This is characterized by a mobilization factor m. Shear resistance of soil is taken as:

Table 1: Notation used in this paper

Parameter	Description
b , C	Width of footing and Cohesive force, respectively
D_e	Distance of the edge of the footing from the slope shoulder
D_f, q	Depth of foundation and load intensity, respectively
$N_{\gamma e}$	Optimized seismic bearing capacity coefficient
m, P_p	Mobilization factor and Passive pressure, respectively
P_{pc}, P_{pq}, $P_{p\gamma}$	Passive pressure corresponding to cohesive, surcharge, and unit weight, respectively
P_{pmc}, P_{pmq}, $P_{pm\gamma}$	Mobilize Passive pressure corresponding to cohesive, surcharge, and unit weight, respectively
β	Angle which the slope makes with the horizontal
θ	log-spiral angle on the slope side
r_0, r	Initial and final radius of the log-spiral, respectively
t, T_s, T_p	Time, and periods of shaking corresponding to shear and pressure waves, respectively
P_L	Uniformly distributed column load
K_h, K_v	Horizontal and vertical seismic accelerations, respectively
V_p,V_s	Primary and shear wave velocities, respectively
α_1, α_2	Base angles of triangular elastic zone under the foundation
Q_v, Q_h	Vertical and Horizontal inertial forces acting on ABN
Q_{v1}, Q_{h1}	Vertical and Horizontal inertial forces acting on AND
Q_{v2}, Q_{h2}	Vertical and Horizontal inertial forces acting on AFD
Q_{v3}, Q_{h3}	Vertical and Horizontal inertial forces acting on BNK
Q_{v4}, Q_{h4}	Vertical and Horizontal inertial forces acting on BKG
γ, ρ, ν, φ	Unit weight, mass density, Poisson's ratio and friction angle of soil, respectively
ω_s, ω_p, λ, η	angular frequency of shear waves, angular frequency of primary waves, wavelength of the shear and primary waves, respectively
M_i	The moment of typical force *i* about the centre of log-spiral

$$\tau = m(c + б\ tan\varphi) \tag{2-4}$$

Virtual rupture wedge ANDE involves a radial shear zone AND and Rankine passive zone ADE delimited by a logarithmic spiral curve ND. Similar to logarithmic spiral curve NK, the equation of ND can be expressed as follows:

$$AD = r_0 e^{\theta_m tan\varphi_m} \tag{2-5}$$

Where,

$$r_0 = AN = \frac{b\ sin\ \alpha_1}{sin(\alpha_1 + \alpha_2)} \tag{2-6}$$

Under earthquake condition, according to Fig. 1 the shear wave with velocity V_s and primary wave with velocity V_p are assumed to propagate within soil medium. The horizontal and vertical sinusoidal accelerations with angular frequency of $\omega=2\pi/T$ at any depth of z below the ground surface can be expressed as follows:

$$a_h(z,t) = K_h g \sin\omega_s(t - \frac{H - z}{V_S}) \tag{2-7}$$

$$a_v(z,t) = K_v g \sin\omega_p(t - \frac{H-z}{V_P}) \quad (2\text{-}8)$$

2.1 Pseudo-dynamic forces acting on the elastic wedge ABN

Fig. 2 illustrates the wedge of ABN and forces acting on AB, AN, and BN. The expression for bearing capacity can be derived by considering the equilibrium of elastic wedge ABN. The forces acting on the elastic wedge include earth pressure P_p and P_{pm} on sides BN and AN; cohesion forces C_a and C_{am} acting on BN and AN; horizontal and vertical inertia forces $Q_{h,ABN}$ and $Q_{v,ABN}$ and finally uniformly distributed vertical load P_L. The mass of the thin elemental slice of thickness dz at a depth of z from the ground surface in elastic wedge ABN can be obtained as:

$$m_{ABN}(z) = \frac{\gamma}{g}\left(\frac{1}{\tan\alpha_1} + \frac{1}{\tan\alpha_2}\right)(r_0 \sin\alpha_1 - z)dz \quad (2\text{-}9)$$

Therefore, the weight of ABN wedge can be calculated as:

$$W = \frac{b^2\gamma}{2}\frac{\sin\alpha_1 \sin\alpha_2}{\sin(\alpha_1+\alpha_2)} \quad (2\text{-}10)$$

Total horizontal and vertical inertia forces $Q_{h,ABN}$ and $Q_{v,ABN}$ acting on the failure wedge ABN can be derived as:

$$Q_h = \int_0^{r_0 sin\alpha_1} m_{ABN}(z)a_h(z,t)dz = \frac{\gamma b^2 \lambda K_h \sin^2\alpha_1 \sin^2\alpha_2}{2\pi r_0 sin\,\alpha_1 \sin^2(\alpha_1+\alpha_2)}\left(\frac{1}{\tan\alpha_1}+\frac{1}{\tan\alpha_2}\right)\times \left[cos\,2\pi\left(\frac{t}{T_s} - \frac{r_0 \sin\alpha_1}{\lambda}\right) + \frac{r_0 sin\,\alpha_1}{2\pi\lambda}\left\{sin\,2\pi\left(\frac{t}{T_s} - \frac{r_0 sin\,\alpha_1}{\lambda}\right) - sin2\pi\frac{t}{T_s}\right\}\right] \quad (2\text{-}11)$$

$$Q_v = \int_0^{r_0 sin\alpha_1} m_{ABN}(z)a_v(z,t)dz = \frac{\gamma b^2 \eta K_v \sin^2\alpha_1 \sin^2\alpha_2}{2\pi r_0 sin\,\alpha_1 \sin^2(\alpha_1+\alpha_2)}\left(\frac{1}{\tan\alpha_1}+\frac{1}{\tan\alpha_2}\right)\times \left[cos\,2\pi\left(\frac{t}{T_p} - \frac{r_0 \sin\alpha_1}{\eta}\right) + \frac{r_0 sin\,\alpha_1}{2\pi\eta}\left\{sin\,2\pi\left(\frac{t}{T_p} - \frac{r_0 sin\,\alpha_1}{\eta}\right) - sin2\pi\frac{t}{T_p}\right\}\right] \quad (2\text{-}12)$$

The seismic passive resistance forces P_p and P_{pm} can be computed as

$$P_p = P_{p\gamma} + P_{pq} + P_{pc} \quad (2\text{-}13)$$

$$P_{pm} = P_{pm\gamma} + P_{pmq} + P_{pmc} \quad (2\text{-}14)$$

From the vertical equilibrium of all the forces acting on the triangular elastic wedge ABN, ultimate vertical failure loads, P_L, can be obtained as follows:

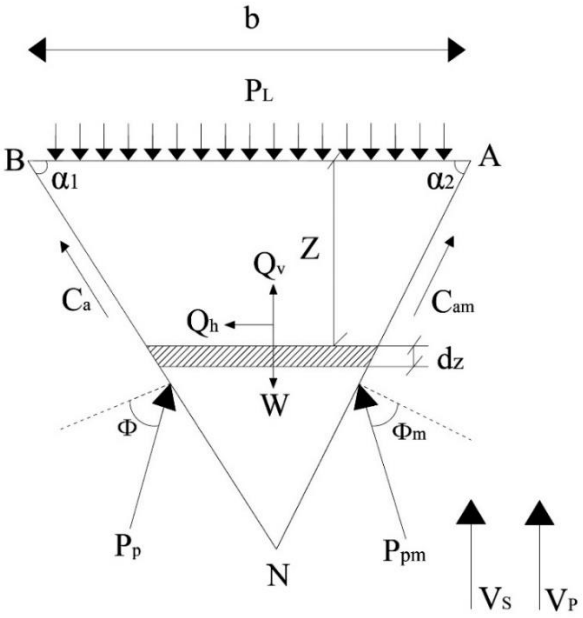

Figure 2: The forces acting on elastic wedge

$$P_L = \frac{P_p\, cos\,(\alpha_1 - \varphi) + P_{pm}\, cos(\alpha_2 - \varphi_m) - W + Q_v}{b} + \frac{c\, sin\,\alpha_1\, sin\,\alpha_2\,(1+m)}{sin(\alpha_1 + \alpha_2)} \tag{2-15}$$

It is noted that m or ϕ_m are unknown that can be determined with iteration technique. By choosing a value for ϕ_m from 0 to ϕ, the trial and error procedure continues until equilibrium of wedge ABN is achieved.

2.2 Pseudo-dynamic forces acting on the soil masses AFDN and BNKG

Soil mass wedges in Fig. 1, are divided into two parts: the forces acting on wedge AFEDN on the side of level ground and the forces acting on downslope wedge BNKG on the left side of point N. The details of the computation of inertial forces acting on AFDN and BNKG are shown in Figs. 3-4, respectively.

Refereeing to Fig. 3 the total horizontal and vertical inertial forces acting on the wedge AFD can be obtained as:

$$Q_{h2} = \int_0^{FD} m_2(z)\, a_h(z,t)\, dz = \frac{\gamma b \lambda K_h \sin\alpha_1 \cos X_m\, e^{\theta_m \tan\varphi_m}}{2\pi \sin(\alpha_1+\alpha_2)} \times \left[\cos 2\pi\left(\frac{t}{T_s}-\frac{FD}{\lambda}\right)+\frac{\lambda}{2\pi FD}\left\{\sin 2\pi\left(\frac{t}{T_s}-\frac{FD}{\lambda}\right)-\sin 2\pi\,\frac{t}{T_s}\right\}\right] \quad (2\text{-}16)$$

$$Q_{v2} = \int_0^{FD} m_2(z)\, a_v(z,t)\, dz = \frac{\gamma b \eta K_v \sin\alpha_1 \cos X_m\, e^{\theta_m \tan\varphi_m}}{2\pi \sin(\alpha_1+\alpha_2)} \times \left[\cos 2\pi\left(\frac{t}{T_p}-\frac{FD}{\eta}\right)+\frac{\eta}{2\pi FD}\left\{\sin 2\pi\left(\frac{t}{T_p}-\frac{FD}{\eta}\right)-\sin 2\pi\frac{t}{T_p}\right\}\right] \quad (2\text{-}17)$$

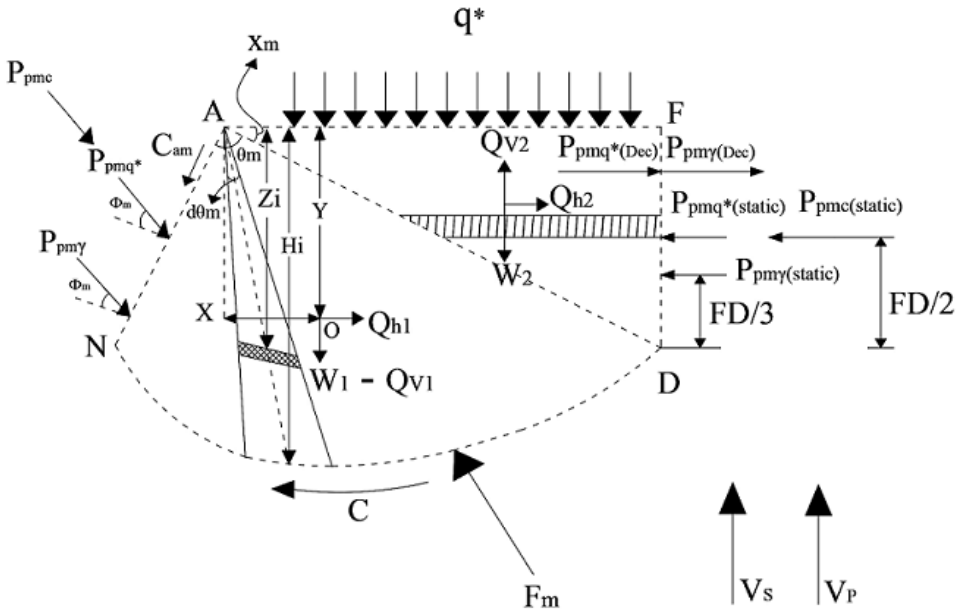

Figure 3: The forces acting on passive AFDN wedge

Where $m_2(z)$ the mass slice of thickness dz in the failure wedge AFD is given by:

$$m_2(z) = \frac{\gamma}{g}\frac{(FD-z)}{\tan X_m} dz \quad (2\text{-}18)$$

In equation (18) the term of X_m is defined as follows:

$$X_m = \frac{\pi}{2} - \varphi_m - \xi \quad (2\text{-}19)$$

$$\varphi_m = \tan^{-1}(m \tan\varphi) \quad (2\text{-}20)$$

Where ξ is the included angle between ED and ground surface can be obtained as

$$\xi = \frac{\pi}{4} - \frac{\varphi_m}{2} + \frac{1}{2}tan^{-1}\left(\frac{K_h}{1-K_v}\right) - \frac{1}{2}sin^{-1}\left[\frac{sin\left\{tan^{-1}(\frac{K_h}{1-K_v})\right\}}{\sin\varphi_m}\right] \quad (2\text{-}21)$$

The passive earth pressure $P_{pmq^*(Dec)}$, and $P_{pm\gamma(Dec)}$ acting on FD can be obtained as

$$P_{pmq^*(Dec)} = \frac{1}{2}H^2\gamma K_{P(Dec)} \quad (2\text{-}22)$$

$$P_{pm\gamma(Dec)} = \frac{1}{2}H^2\gamma K_{P(Dec)} \quad (2\text{-}23)$$

Where

$$K_{P(Dec)} = (1 + sin\Phi_m)/(1 - sin\Phi_m) \quad (2\text{-}24)$$

The total horizontal and vertical inertia forces $(Q_{h1})_i$ and $(Q_{v1})_i$ within i^{th} slice of the failure wedge ADN can be expressed as follows:

$$(Q_{h1})_i = \int_0^{H_i} m_1(z)_i \; a_h(z,t)_i \; (dz)_i = \frac{\gamma K_h \lambda \, d\theta_m \, {r_0}^2\left(e^{(i-1)d\theta_m \, tan\varphi_m} + e^{i \, d\theta_m \tan\varphi_m}\right)}{360^0 * 4H_i} \times \left[\frac{\lambda}{2\pi H_i}\left\{sin2\pi\frac{t}{T_s} - \sin 2\pi\left(\frac{t}{T_s} - \frac{H_i}{\lambda}\right)\right\} - \cos 2\pi\left(\frac{t}{T_s}\right)\right] \quad (2\text{-}25)$$

$$(Q_{v1})_i = \int_0^{H_i} m_1(z)_i \; a_v(z,t)_i \; (dz)_i = \frac{\gamma K_v \, \eta \, d\theta_m \, {r_0}^2\left(e^{(i-1)d\theta_m \, tan\varphi_m} + e^{i \, d\theta_m \tan\varphi_m}\right)}{360^0 * 4H_i} \times \left[\frac{\eta}{2\pi H_i}\left\{sin2\pi\frac{t}{T_p} - \sin 2\pi\left(\frac{t}{T_p} - \frac{H_i}{\eta}\right)\right\} - \cos 2\pi\left(\frac{t}{T_p}\right)\right] \quad (2\text{-}26)$$

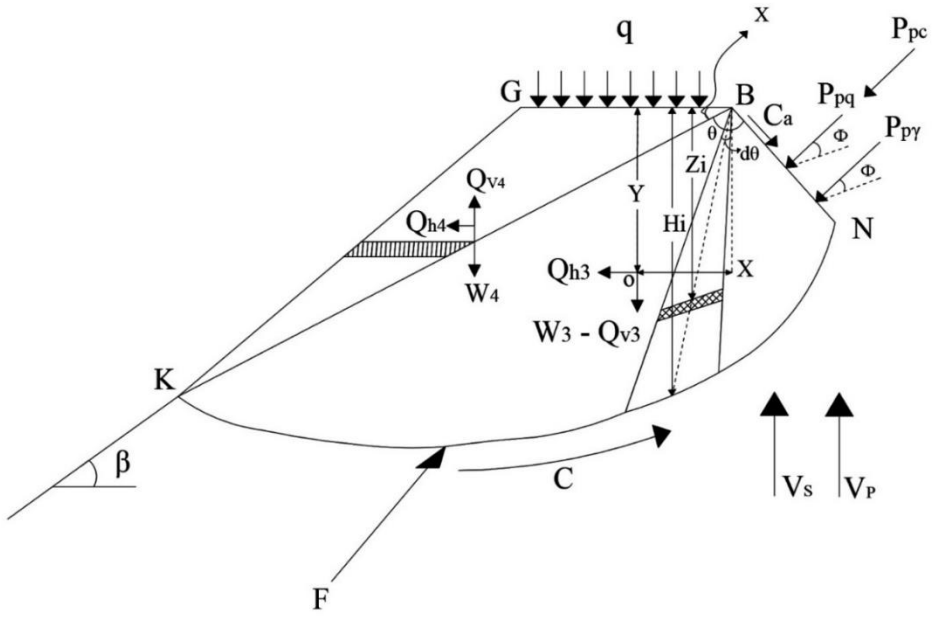

Figure 4: The forces acting on passive BNKG wedge

The mass of the elemental i^{th} slice of thickness dz at depth z in the virtual failure wedge AND, is given by:

$$m_1(z)_i = \frac{\gamma}{g}\frac{2\pi\, d\theta_m}{360^0 sin^2(\alpha + (i-0.5)d\theta_m)}\int_0^{H_i} z_i(dz)_i \tag{2-27}$$

Referring to Fig. 4 the total horizontal and vertical inertial forces acting on the wedge BGK can be obtained as:

$$Q_{h4} = \int_0^{BK\ sinX} m_4(z)\ a_h(z,t)\ dz = \frac{\gamma b\lambda K_h\ sin\alpha_2\ \ \sin X\ \ (\cot X - \cot\beta)e^{\theta tan\varphi}}{4\pi^2 \sin(\alpha_1+\alpha_2)} \times \left[2\pi\ \cos 2\pi\left(\frac{t}{T_s} - \frac{BK\ sinX}{\lambda}\right) + \frac{\lambda}{BK\ sinX}\left\{\sin 2\pi\left(\frac{t}{T_s} - \frac{BK\ sinX}{\lambda}\right) - sin2\pi\frac{t}{T_s}\right\}\right] \tag{2-28}$$

$$Q_{v4} = \int_0^{BK\ sinX} m_4(z)\ a_v(z,t)\ dz = \frac{\gamma b\eta K_v\ sin\alpha_2\ \ \sin X\ \ (\cot X - \cot\beta)e^{\theta tan\varphi}}{4\pi^2 \sin(\alpha_1+\alpha_2)} \times \tag{2-29}$$

$$\left[2\pi\cos 2\pi\left(\frac{t}{T_p}-\frac{BK\,sinX}{\eta}\right)+\frac{\eta}{BK\,sinX}\left\{\sin 2\pi\left(\frac{t}{T_p}-\frac{BK\,sinX}{\eta}\right)-sin2\pi\frac{t}{T_p}\right\}\right]$$

Where $m_4(z)$ the mass slice of thickness dz in the failure wedge BKG is given by:

$$m_4(z)=\frac{\gamma(BK\,sinX-z)(\cot\alpha-\cot\beta)}{g}\,dz \tag{2-30}$$

The total horizontal and vertical inertia forces $(Q_{h3})_i$ and $(Q_{v3})_i$ within i^{th} slice of the failure wedge BNK can be expressed as follow:

$$\begin{aligned}(Q_{h3})_i&=\int_0^{H_i} m_3(z)_i\;a_h(z,t)_i\;(dz)_i\\&=\frac{\gamma K_h\,\lambda\,d\theta\,{r_0}^2\left(e^{(i-1)d\theta\,tan\varphi}+e^{i\,d\theta\tan\varphi}\right)}{360^0*4H_i}\\&\times\left[\frac{\lambda}{2\pi H_i}\left\{sin2\pi\frac{t}{T_s}-\sin 2\pi\left(\frac{t}{T_s}-\frac{H_i}{\lambda}\right)\right\}-\cos2\pi\left(\frac{t}{T_s}\right)\right]\end{aligned} \tag{2-31}$$

$$\begin{aligned}(Q_{v3})_i&=\int_0^{H_i} m_3(z)_i\;a_v(z,t)_i\;(dz)_i\\&=\frac{\gamma K_v\,\eta\,d\theta\,{r_0}^2\left(e^{(i-1)d\theta\,tan\varphi}+e^{i\,d\theta\tan\varphi}\right)}{360^0*4H_i}\\&\times\left[\frac{\eta}{2\pi H_i}\left\{sin2\pi\frac{t}{T_p}-\sin 2\pi\left(\frac{t}{T_p}-\frac{H_i}{\eta}\right)\right\}-\cos2\pi\left(\frac{t}{T_p}\right)\right]\end{aligned} \tag{2-32}$$

The mass of the elemental i^{th} slice of thickness dz at depth z in the realistic failure wedge BNK, is given by:

$$m_3(z)_i=\frac{\gamma}{g}\,\frac{2\pi\,d\theta}{360^0 sin^2(\alpha+(i-0.5)d\theta)}\int_0^{H_i} z_i(dz)_i \tag{2-33}$$

2.3 Passive Earth Pressure Forces $P_{p\gamma}$, P_{pq} and P_{pc} Acting on BNKG

Passive earth pressure P_p which consists of three components $P_{p\gamma}$, P_{pq} , and P_{pc}. $P_{p\gamma}$ represents the resistance due to the weight of the soil mass BNKG. P_{pq} and P_{pc} represent the resistance due to surcharge loading and the soil cohesion, respectively. The point of application of $P_{p\gamma}$ is placed at two-third position of BN. Both P_{pq} and P_{pc} are uniformly distributed and their point of application is placed at the midpoint of BN. Resultant F of normal and frictional forces acting on surface of NK must be toward the point B. Cohesive forces C and C_a act along NK and BN, respectively. The surcharge intensity, q, on the side of the slope has been expressed as

$$q = \frac{D_e \gamma\, D_f \tan\beta + \frac{1}{2}\,\gamma\, {D_f}^2}{D_e \tan\beta + D_f} \tag{2-34}$$

Hijab (1956) [8] presented a formulation for calculating the centroid of the log spiral shear zone BNK. As delineated in Fig.4, *OX* and *OY* which are the horizontal and vertical distance of the centroid of the gravity, point O, from the center of the log spiral, point B, can be obtained as:

$$OX = \frac{4}{3} r_0 \frac{\tan\varphi}{(1+9tan^2\varphi)(e^{2\theta\, tan\varphi}-1)} \times \begin{bmatrix} \{e^{3\theta\, tan\varphi}(3\tan\varphi\sin\theta - \cos\theta)+1\}\sin\alpha_2 \\ -\{e^{3\theta\, tan\varphi}, -3\tan\varphi\sin\theta - \cos\theta\}\cos\alpha_2 \end{bmatrix} \tag{2-35}$$

$$OY = \frac{4}{3} r_0 \frac{\tan\varphi}{(1+9tan^2\varphi)(e^{2\theta\, tan\varphi}-1)} \times \begin{bmatrix} \{e^{3\theta\, tan\varphi}(3\tan\varphi\sin\theta - \cos\theta)+1\}\cos\alpha_2 \\ +\{e^{3\theta\, tan\varphi} - 3\tan\varphi\sin\theta - \cos\theta\}\sin\alpha_2 \end{bmatrix} \tag{2-36}$$

Taking Moment equilibrium due to weight of the soil mass about the focus *B*, yields $P_{p\gamma}$

$$M_{P_{p\gamma}} = M_{W_3} + M_{W_4} - M_{Q_{h4}} - M_{Q_{h3}} - M_{Q_{v3}} - M_{Q_{v4}} \tag{2-37}$$

thus,

$$\mathrm{P_{p\gamma}} = a_1[a_2(a_3 - a_4) + a_5 - a_6(a_7 + a_8)] \tag{2-38}$$

In which,

$$a_1 = \frac{\gamma}{2} b^2 \frac{sin^2{}_{\alpha_2}}{2\, cos\varphi\, sin^2\,(\alpha_1+\alpha_2)} \tag{2-39}$$

$$a_2 = e^{3\theta\tan\varphi}\, sinX \tag{2-40}$$

$$a_3 = cos^2X - \frac{K_h\,\lambda\,(cotX - cot\beta)}{\pi^2\, BK} \times \left[2\pi\, cos2\pi\left(\frac{t}{T_s} - \frac{BK\, sinX}{\lambda}\right) + \frac{\lambda}{BK\, sinX}\left\{sin2\pi\left(\frac{t}{T_s} - \frac{BK\, sinX}{\lambda}\right) - sin2\pi\frac{t}{T_s}\right\}\right] \tag{2-41}$$

$$a_4 = \frac{2K_v\eta\,(cotX - cot\beta)\, cosX}{\pi^2\, BK\, sinX} \times \left[2\pi\, cos2\pi\left(\frac{t}{T_p} - \frac{BK\, sinX}{\eta}\right) + \frac{\eta}{BK\, sinX}\left\{sin2\pi\left(\frac{t}{T_p} - \frac{BK\, sinX}{\eta}\right) - sin2\pi\frac{t}{T_p}\right\}\right] \tag{2-42}$$

$$a_5 = \frac{2}{(1+9tan^2\varphi)}\begin{bmatrix} \{e^{3\theta\, tan\varphi}(3\tan\varphi\sin\theta - \cos\theta)+1\}sin\,\alpha_2 \\ -\{e^{3\theta\, tan\varphi} - 3\tan\varphi\sin\theta - \cos\theta\}\cos\alpha_2 \end{bmatrix} \tag{2-43}$$

$$a_6 = \frac{2d\theta\, tan\varphi\, \sum_{i=1}^{n}(e^{(i-1)d\theta\, tan\varphi} + e^{i\, d\theta\, tan\varphi})^2}{360^0\,(1+9\tan^2\varphi\,)\,(e^{2\,\theta\, tan\varphi}-1)} \tag{2-44}$$

$$a_7 = \frac{\lambda K_h}{H_i}\left[\frac{\lambda}{2\pi\, H_i}\left\{sin2\pi\frac{t}{T_s} - sin2\pi\left(\frac{t}{T_s} - \frac{H_i}{\lambda}\right)\right\} - cos2\pi\frac{t}{T_s}\right]\left[\begin{matrix}\left\{e^{3\theta\, tan\varphi}(3\tan\varphi\sin\theta - \cos\theta) + 1\right\}\cos\alpha_2 \\ +\left\{e^{3\theta\, tan\varphi} - 3\tan\varphi\sin\theta - \cos\theta\right\}\sin\alpha_2\end{matrix}\right] \quad (2\text{-}45)$$

$$a_8 = \frac{\eta\, K_v}{H_i}\left[\frac{\eta}{2\pi\, H_i}\left\{sin2\pi\frac{t}{T_p} - sin2\pi\left(\frac{t}{T_p} - \frac{H_i}{\eta}\right)\right\} - cos2\pi\frac{t}{T_p}\right]\left[\begin{matrix}\left\{e^{3\theta\, tan\varphi}(3\tan\varphi\sin\theta - \cos\theta) + 1\right\}\sin\alpha_2 \\ -\left\{e^{3\theta\, tan\varphi} - 3\tan\varphi\sin\theta - \cos\theta\right\}\cos\alpha_2\end{matrix}\right] \quad (2\text{-}46)$$

Taking Moment equilibrium due to surcharge loading and soil cohesion, yields P_{pq} as:

$$M_{P_{pq}} = M_q \quad (2\text{-}47)$$

$$P_{Pq} = \frac{\gamma}{2}b^2\left(\frac{D_e}{b} + \frac{1}{2}\frac{D_f}{b\, tan\beta}\right)\frac{2\, sin\alpha_2}{sin(\alpha_1 + \alpha_2)cos\varphi}\left(e^{2\theta\, tan\varphi}\right)cos^2 x \quad (2\text{-}48)$$

Similarly by moment equilibrium due to soil cohesion P_{pc} can be obtained as:

$$M_{P_{pc}} = M_c \quad (2\text{-}49)$$

$$P_{pc} = \frac{\gamma}{2}b^2\frac{4c}{\gamma b}\frac{sin\alpha_2}{cos\varphi\, sin(\alpha_1 + \alpha_2)}\frac{\left(e^{2\theta\, tan\varphi} - 1\right)}{tan\varphi} \quad (2\text{-}50)$$

Finally the value of P_p can be calculated:

$$P_p = P_{p\gamma} + P_{pq} + P_{pc} \quad (2\text{-}13)$$

2.4 Passive Earth Pressure Forces $P_{pm\gamma}$, P_{pmq^*} and P_{pmc} Acting on AFEDN

In a similar manner, passive earth pressure P_{pm} at partial mobilization m can be divided into three component $P_{pm\gamma}$, P_{pmq*}, and P_{pmc} representing the resistance due to weight, surcharge and cohesion of the soil mass AFDN, respectively (Fig. 3). Resultant, F_m,of normal and frictional forces acting on the surface of ND must be directed toward the point A. Cohesive forces C and C_{am} acting along ND and AN, respectively. The surcharge intensity q^* on the side of level ground has been expressed as:

$$q^* = \gamma D_f \quad (2\text{-}51)$$

Taking moment equilibrium due to weight of the soil mass, surcharge loading and soil cohesion about the focus A, yields $P_{pm\gamma}$, P_{pmq*}, and P_{pmc} respectively:

$$P_{pm\gamma} = b_1[b_2(b_3 - b_4) + b_5 - b_6(b_7 + b_8)] \quad (2\text{-}52)$$

$$P_{pmq^*} = \frac{\gamma}{2}b^2\,\frac{D_f}{b}\,\frac{2\sin\alpha_1\cos X_m\; e^{2\theta_m\tan\varphi_m}}{\cos\varphi_m\sin(\alpha_1 + \alpha_2)} \times \left[\cos X_m + \sin X_m\left\{1 - \frac{2}{3}\,K_{p_{(Dec)}}\right\}\right] \quad (2\text{-}53)$$

$$P_{pmc} = \frac{\gamma}{2}b^2\frac{2c}{\gamma b}\frac{\sin\alpha_1}{\cos\varphi_m\sin(\alpha_1 + \alpha_2)} \times$$

$$\left[\frac{(e^{2\theta_m \tan\varphi_m}-1)}{\tan\varphi_m}+e^{2\theta_m \tan\varphi_m}\sin^2 x_m\right] \quad (2\text{-}54)$$

In which,

$$b_1=\frac{\gamma}{2}b^2\frac{\sin^2\alpha_1}{2\cos\Phi_m\sin^2(\alpha_1+\alpha_2)} \quad (2\text{-}55)$$

$$b_2=e^{3\theta_m\tan\Phi_m}\cos X_m\sin X_m \quad (2\text{-}56)$$

$$b_3=2\cos X_m+2\sin X_m-\frac{K_h\lambda\sin X_m}{\pi FD}\times \left[\cos 2\pi\left(\frac{t}{T_s}-\frac{FD}{\lambda}\right)+\frac{\lambda}{2\pi FD}\left\{\sin 2\pi\left(\frac{t}{T_s}-\frac{FD}{\lambda}\right)-\sin 2\pi\frac{t}{T_s}\right\}\right] \quad (2\text{-}57)$$

$$b_4=\frac{2K_v\eta\cos X_m}{\pi FD}\left[\begin{matrix}\cos 2\pi\left(\frac{t}{T_p}-\frac{FD}{\eta}\right)\\ +\frac{\eta}{2\pi FD}\left\{\sin 2\pi\left(\frac{t}{T_p}-\frac{FD}{\eta}\right)-\sin 2\pi\frac{t}{T_p}\right\}\end{matrix}\right] -\sin X_m K_{p_{(Dec)}} \quad (2\text{-}58)$$

$$b_5=\frac{2}{(1+9\tan^2\Phi_m)}\left[\left\{e^{3\theta_m\tan\Phi_m}(3\tan\Phi_m\sin\theta_m-\cos\theta_m)+1\right\}\sin\alpha_1 -\left\{e^{3\theta_m\tan\Phi_m}-3\tan\Phi_m\sin\theta_m-\cos\theta_m\right\}\cos\alpha_1\right] \quad (2\text{-}59)$$

$$b_6=\frac{2d\theta_m\tan\Phi_m\sum_{i=1}^{n}(e^{(i-1)d\theta_m\tan\Phi_m}+e^{i\,d\theta_m\tan\Phi_m})^2}{360^0(1+9\tan^2\Phi_m)(e^{2\theta_m\tan\Phi_m}-1)} \quad (2\text{-}60)$$

$$b_7=\frac{\lambda K_h}{H_i}\left[\frac{\lambda}{2\pi H_i}\left\{\sin 2\pi\frac{t}{T_s}-\sin 2\pi\left(\frac{t}{T_s}-\frac{H_i}{\lambda}\right)\right\}-\cos 2\pi\frac{t}{T_s}\right] \left[\begin{matrix}\left\{e^{3\theta_m\tan\Phi_m}(3\tan\Phi_m\sin\theta_m-\cos\theta_m)+1\right\}\cos\alpha_1\\ +\left\{e^{3\theta_m\tan\Phi_m}-3\tan\Phi_m\sin\theta_m-\cos\theta_m\right\}\sin\alpha_1\end{matrix}\right] \quad (2\text{-}61)$$

$$b_8=\frac{\eta K_v}{H_i}\left[\frac{\eta}{2\pi H_i}\left\{\sin 2\pi\frac{t}{T_p}-\sin 2\pi\left(\frac{t}{T_p}-\frac{H_i}{\eta}\right)\right\}-\cos 2\pi\frac{t}{T_p}\right]\times \left[\begin{matrix}\left\{e^{3\theta_m\tan\Phi_m}(3\tan\Phi_m\sin\theta_m-\cos\theta_m)+1\right\}\sin\alpha_1\\ -\left\{e^{3\theta_m\tan\Phi_m}-3\tan\Phi_m\sin\theta_m-\cos\theta_m\right\}\cos\alpha_1\end{matrix}\right] \quad (2\text{-}62)$$

Therefore the value of P_{pm} can be obtained as:

$$P_{pm}=P_{pm\gamma}+P_{pmq^*}+P_{pmc} \quad (2\text{-}14)$$

Now, by substituting Eqs. (2-10), (2-12), (2-13) and (2-14) into Eq. (2-15), failure load, P_L acting on the foundation can be calculated. The seismic bearing capacity coefficient, $N_{\gamma e}$, for strip footing placed adjacent to the slope can be obtained as

$$N_{\gamma e}=\frac{2\mathrm{P_L}}{\gamma b} \quad (2\text{-}63)$$

$$N_{\gamma E} = c_1[a_2(a_3 - a_4) + a_5 - a_6(a_7 + a_8) + c_2] + c_3[b_2(b_3 - b_4) + b_5 - b_6(b_7 + b_8) + c_4] + c_5 \quad (2\text{-}64)$$

In which,

$$c_1 = \frac{\cos(\alpha_1 - \varphi)\, sin^2\, \alpha_2}{2\, cos\varphi\, sin^2\, (\alpha_1 + \alpha_2)} \quad (2\text{-}65)$$

$$c_2 = \left(\frac{D_e}{b} + \frac{1}{2}\frac{D_f}{b\, tan\beta}\right)\frac{4sin(\alpha_1 + \alpha_2)}{sin\alpha_2}\left(e^{2\theta\, tan\varphi}\right)cos^2 x + \frac{2c}{\gamma b}\,\frac{4sin(\alpha_1 + \alpha_2)}{sin\alpha_2}\,\frac{\left(e^{2\theta\, tan\varphi} - 1\right)}{tan\varphi} \quad (2\text{-}66)$$

$$c_3 = \frac{\cos(\alpha_2 - \varphi_m)\, sin^2\, \alpha_1}{2\, cos\varphi_m\, sin^2\, (\alpha_1 + \alpha_2)} \quad (2\text{-}67)$$

$$c_4 = \frac{D_f}{b}\,\frac{4\sin(\alpha_1 + \alpha_2)\cos X_m\; e^{2\theta_m \tan\varphi_m}}{\sin\alpha_1} \times \left[\cos X_m + sin\, X_m\left\{1 - \frac{2}{3}\, K_{p_{(Dec)}}\right\}\right] + \frac{2c}{\gamma b}\,\frac{2\sin(\alpha_1 + \alpha_2)}{\sin\alpha_1} \times \left[\frac{(e^{2\theta_m\, tan\varphi_m} - 1)}{\tan\varphi_m} + e^{2\theta_m\, tan\varphi_m} sin^2\, X_m\right] \quad (2\text{-}68)$$

$$c_5 = \frac{sin\alpha_1\, sin\alpha_2}{\sin(\alpha_1 + \alpha_2)}\left[-1 + c(1 + m) + \frac{\eta K_v \sin\alpha_1\, \sin\alpha_2}{\pi r_0 sin\, \alpha_1 \sin(\alpha_1 + \alpha_2)}\left(\frac{1}{tan\, \alpha_1} + \frac{1}{\tan\alpha_2}\right) \times \left[cos2\pi\left(\frac{t}{T_p} - \frac{r_0\, sin\, \alpha_1}{\eta}\right) + \frac{r_0 sin\, \alpha_1}{2\pi\eta}\left\{\sin 2\pi\left(\frac{t}{T_p} - \frac{r_0 sin\, \alpha_1}{\eta}\right) - sin2\pi\frac{t}{T_p}\right\}\right]\right] \quad (2\text{-}69)$$

3 Results and Discussion

The main result of this study is the formulation of seismic bearing capacity factor, Nγe that presented in Eq. 2-64 as a function of seismic acceleration coefficients, slope angle, t/T, friction angle, and cohesion. Since the seismic bearing capacity coefficient Nγe for the simultaneous resistance of surcharge, unit weight and cohesion is calculated, the ultimate seismic bearing capacity of shallow foundations resting on C-φ soil which are adjacent to slopes can be directly calculated from Eq. 63 without the need to calculate Nce or Nqe.

The Eq. 63 is applied to some typical data set to demonstrate its application in calculation of the seismic bearing capacity of shallow strip footing adjacent to slope. Variations of different parameters considered in the present analysis are as follows: φ=20,30 and 40°; β= 10, 20 and 30°; K_h=0.1, 0.2, and 0.3; K_v=0, 0.5 K_h, and K_h;

2c/γb=0, 0.25, and 0.5; D_f/b=0.25, 0.5, and 0.75; D_e/b=0, 1, and 2. The effects of various parameters on the seismic bearing capacity are also described in details as follows.

3.1 Influence of φ on the seismic bearing capacity coefficient

Fig. 5 illustrates the variation in the seismic bearing capacity coefficient, $N_{\gamma e}$ with horizontal seismic acceleration for different soil friction angles (φ=20, 30 and 40°). As expected the bearing capacity coefficient, $N_{\gamma e}$ shows significant increase with an increase in the value of soil friction angle. For K_h = 0.2 the seismic bearing capacity coefficient, $N_{\gamma e}$ increases by approximately 187 and 284% when φ increases from 20 to 30^0 and from 30 to 40^0, respectively.

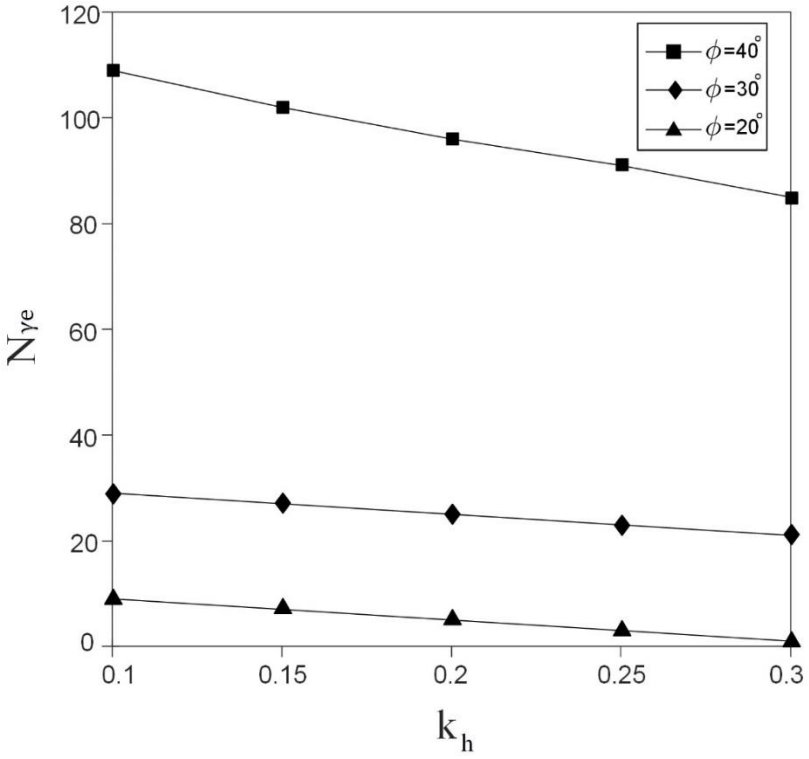

Figure 5: Bearing capacity coefficient vs. horizontal seismic acceleration for different soil friction angles φ (β= 20°, K_v= 0.5 K_h, 2c/γb=0.25, D_f/b=0.5, and D_e/b=0).

3.2 Influence of 2c/γb on the seismic bearing capacity coefficient

Fig. 6 depicts the variation in the seismic bearing capacity coefficient, $N_{\gamma e}$ with horizontal seismic acceleration for different cohesion factors ($2c/\gamma b$=0, 0.25, and 0.5). It can be noticed from Fig. 8 that as expected the bearing capacity coefficient $N_{\gamma e}$ increases with increase in the value of cohesion factor$2c/\gamma b$. considering K_h=0.2, the seismic bearing capacity coefficient, $N_{\gamma e}$ increases by approximately 53 and 106% when$2c/\gamma b$ increases from0 to 0.25 and from 0 to 0.5, respectively.

3.3 Influence of (D_f/b) on the seismic bearing capacity coefficient

Fig. 7 depicts the variation in the seismic bearing capacity coefficient, $N_{\gamma e}$ with horizontal seismic acceleration for different depth factors (D_e/b=0, 1, and 2). It can be observed from Fig. 8 that the bearing capacity coefficient, $N_{\gamma e}$ increases with an increase in the value of depth factor. In other words, the value of surcharge intensity increases with an increase in depth factor, D_f/b .This behaviour is attributed to increased passive resistance and hence the bearing capacity factor increases. The seismic bearing capacity coefficient corresponding to K_h=0.2, increases by approximately 10 and 27% when D_f/b increases from 0.25 to 0.5 and from 0.25 to 1, respectively.

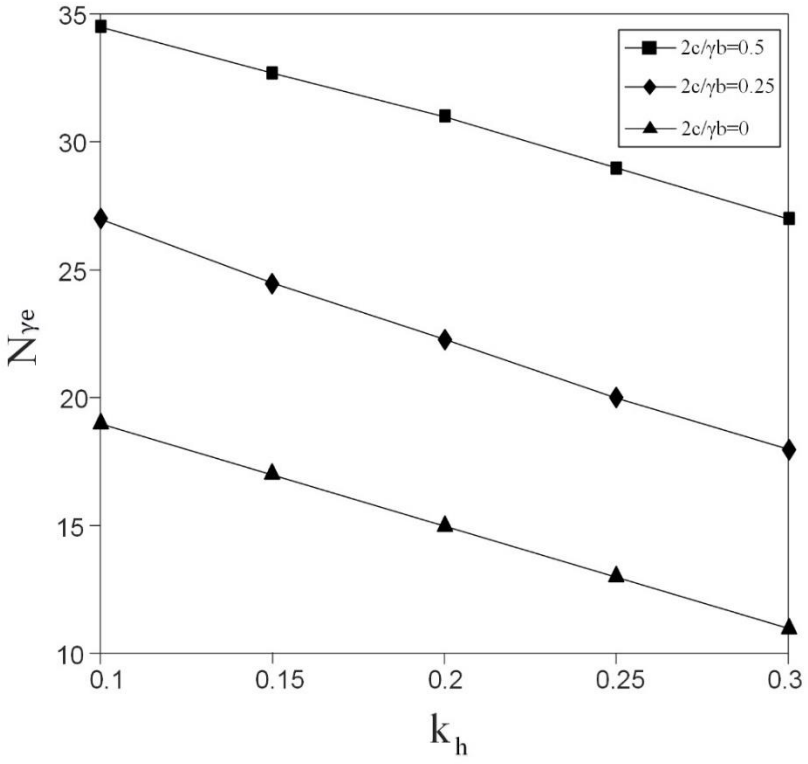

Figure 6: Bearing capacity coefficient vs. horizontal seismic acceleration for different cohesion factors, $2c/\gamma b$ (β= 20°, K_v= 0.5 K_h, D_f/b=0.5, φ= 30° and D_e/b=0).

3.4 Influence of K_v and K_h on the seismic bearing capacity coefficient

Fig. 8 illustrates the variation in the seismic bearing capacity coefficient, $N_{\gamma e}$ with horizontal seismic acceleration K_h for different vertical seismic accelerations (K_v=0, 0.5 K_h, and K_h). From the results presented in Fig. 6, it can be noted that the bearing capacity coefficient, $N_{\gamma e}$ decreases with increase in the intensity of horizontal and vertical seismic acceleration coefficients. For K_h=0.2 the seismic bearing capacity coefficient, $N_{\gamma e}$ increases by approximately 8 and 32% when K_v increases from *0* to *0.5*K_h and from 0 to K_h, respectively.

3.5 Effect of β on the seismic bearing capacity coefficient

Fig. 9 shows the variation of the seismic bearing capacity coefficient, $N_{\gamma e}$ with horizontal seismic acceleration for

different slope angles (β= 10,20 and 30°). The results demonstrate that the bearing capacity coefficient, $N_{\gamma e}$ decreases with increase in slope angle. Due to increase in slope angle the asymmetry of the rupture plane will be increased, which allows the critical failure surface to extend near the foundation and therefore the bearing capacity factor decreases. considering K_h=0.2, the seismic bearing capacity coefficient, $N_{\gamma e}$ increases by approximately 176 and 264% when β increases from 10 to 20° and from 20 to 30°, respectively.

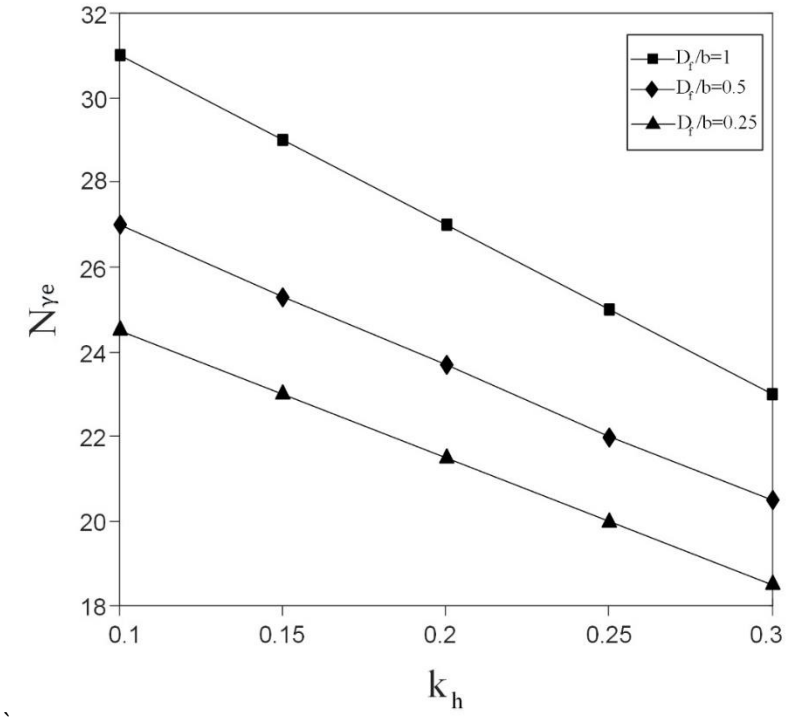

Figure 7: Bearing capacity coefficient vs. horizontal seismic acceleration for different depth factors, D_f/b (β= 20°, K_v= 0.5 K_h, $2c/\gamma b=0.25$, φ= 30° and D_e/b=0).

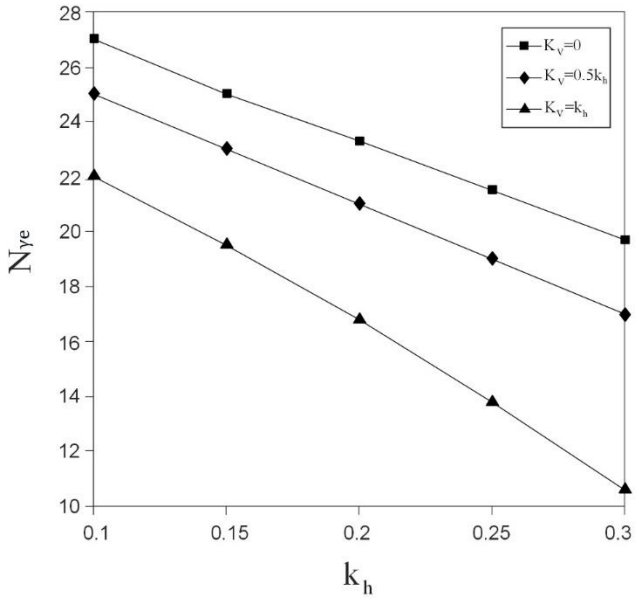

Figure 8: Effect of vertical seismic acceleration on $N_{\gamma e}$ (β= 20°, D_f/b=0.5, $2c/\gamma b=0.25$, φ= 30° and D_e/b=0).

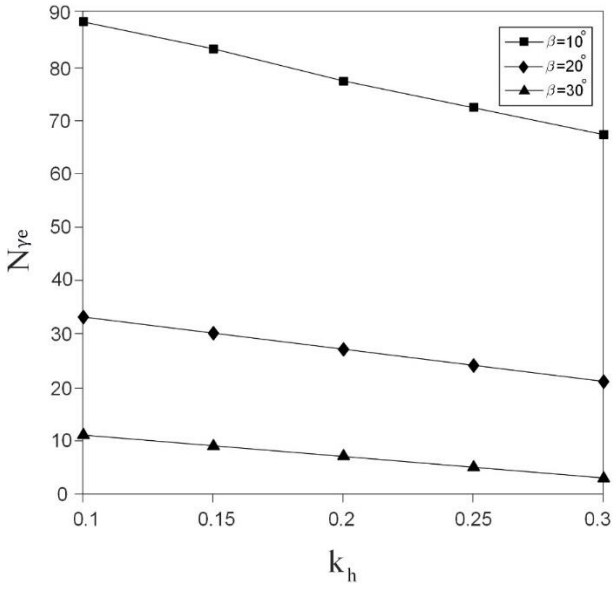

Figure 9: Bearing capacity coefficient vs. horizontal seismic acceleration for different slope angles on β (D_f/b=0.5, $2c/\gamma b=0.25$, φ= 30°, D_e/b=0, and $K_v=0.5K_h$).

3.6 Influence of (D_e/b) on the seismic bearing capacity coefficient

Fig. 10 illustrates the variation in the seismic bearing capacity coefficient, $N_{\gamma e}$ with horizontal seismic acceleration (K_h) for different distance of footing from slope edge factors (D_e/b=0, 1 and 2). It can be observed from Fig. 8 that the bearing capacity coefficient, $N_{\gamma e}$ increases with an increase in the value of distance of footing from slope edge factor (D_e/b). when the footing is placed far away from the slope edge, the slope has no effect on the bearing capacity and hence the bearing capacity factor is obviously increased. The seismic bearing capacity coefficient corresponding to K_h=*0.2*, increases by approximately 16 and 31% when (D_e/b) increases from 0 to 1 and from 0 to 2, respectively.

4 Comparisons

Fig. 11 shows a comparison of seismic bearing capacity coefficient obtained in the current study with the values obtained from the previous pseudo static analyses. No previous study on the seismic bearing capacity of strip footings adjacent to slope using pseudo dynamic approach is available in the literature, therefore a comparison is carried out with the available pseudo-static solutions for bearing capacity of strip footing embedded on slope and located at the edge of a single-side slope (D_e/b=0), and also the available literature on the pseudo-static bearing capacity of strip footing located on horizontal ground surface, e.g., Soubra 1999 [16]; Ghosh and Kumar 2005 [7]; Kumar and Ghosh 2006 [9]; Kumar and Kumar 2003 [10]. The variation of $N_{\gamma e}$ with changes in K_h

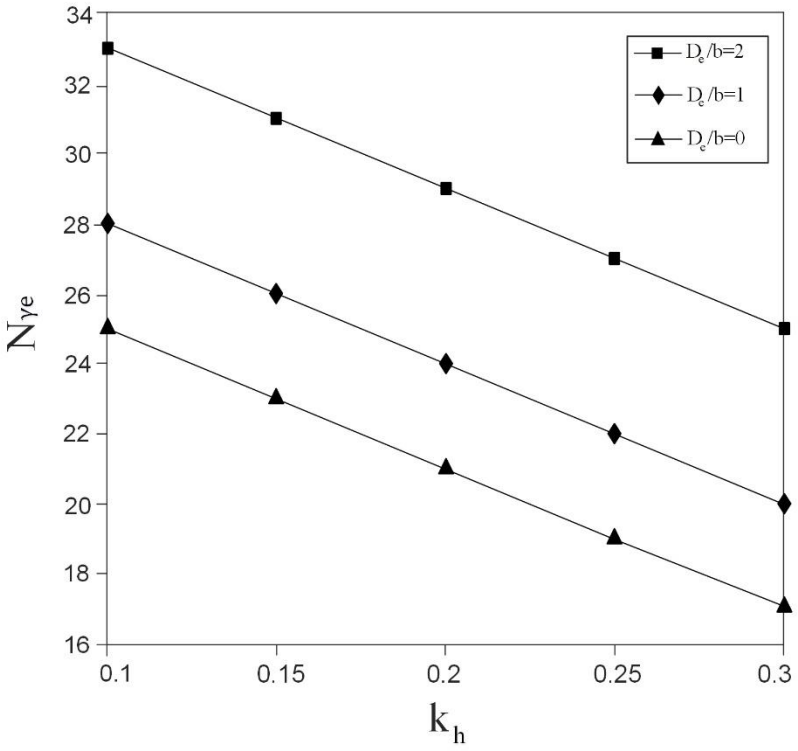

Figure 10: Bearing capacity coefficient vs. horizontal seismic acceleration for different distance of footing from slope edge factors D_e/b (D_f/b=0.5, $2c/\gamma b=0.25$, φ= 30°, β= 20°, and $K_v=0.5K_h$).

obtained from the present study for β= 0 and 20° (φ= 30°, D_e/b=0, D_f/b=0.5) are compared with the solutions given by Soubra (1999) [16], Ghosh and Kumar (2005) [7] and Kumar and Ghosh (2006) [9], who used upper bound limit analysis. It can be noted from Fig. 2 (a, and b) that values of $N_{\gamma e}$ calculated by employing limit equilibrium method are lower than those calculated in previous analytical investigations.

For β= 0 and 20° (φ= 30°, D_e/b=0, D_f/b=3), the variation of $N_{\gamma e}$ with changes in K_h as obtained from present study is compared with solution of Kumar and Kumar (2003) [10] where pseudo-static approach was used to obtain limit equilibrium method considering only horizontal seismic acceleration for foundation embedded on sloping ground. The comparisons of results are presented in Figs. 6 (c, and d), respectively. It can also be noticed that the present analysis provides slightly lower values of $N_{\gamma e}$ as compared with analysis of Kumar and Kumar

(2003) [10]. As a result, one of the main reasons for the existing difference in results may be attributed to the intrinsic differences between upper-bound limit analysis and limit equilibrium methods. Additionally, previous analysis has not considered the influence of pseudo-dynamic loads which makes use of both the horizontal and vertical seismic acceleration coefficients to consider the oscillation of seismic forces.

5 Conclusions

By using pseudo-dynamic approach and applying limit equilibrium method, the seismic bearing capacity of shallow strip footing resting on C-φ which are adjacent to slope were determined. This paper provides a new formulation for computation of seismic bearing capacity coefficient ($N_{\gamma e}$) for the concurrent resistance of surcharge, unit weight and cohesion using two sided composite failure surface for strip footings adjacent to slope considering the effect of time and phase difference in both the shear wave and primary wave velocities Propagating through the soil layer during earthquake. The values obtained from present pseudo-dynamic approach are compared with those of pseudo-static solution given in the literature. It is clear that the pseudo-static loads estimated on basis of a seismic coefficient method cannot predict the oscillatory nature of seismic forces. It can be concluded that the values obtained from present pseudo-dynamic method gives the minimum seismic bearing capacity coefficient than available theories from the literature. A comparison of the proposed method with available pseudo-static results shows the adverse effect of dynamic loading to be considered for the seismic bearing capacity of shallow strip footing.

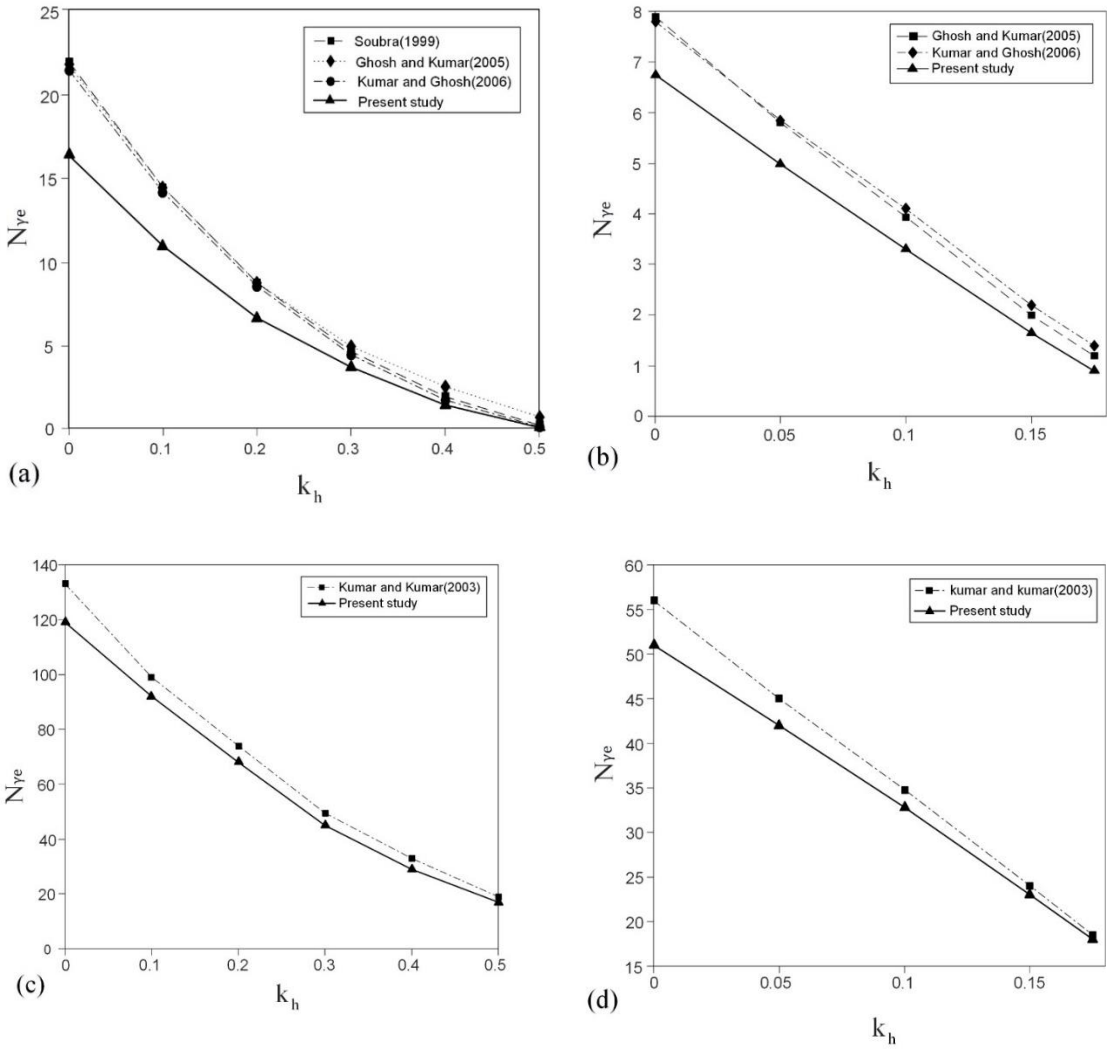

Figure 11: Comparison of $N_{\gamma e}$ with K_h for D_f/b = 0 and 3: (a) φ= 30°, β= 0°, D_f/b=0 ; (b) φ= 30°, β= 20°, D_f/b=0; (c) φ= 30°, β= 0°, D_f/b=3; (d) φ= 30°, β= 20°, D_f/b=3

References

[1] F. Askari, O. Farzaneh, Upper-bound solution for seismic bearing capacity of shallow foundations near slopes, Geotechnique, 53(8) 2003, 697–702.

[2] M. Budhu, A. Al-Karni, Seismic Bearing Capacity of Soils, Geotechnique, 43 (1) 1993, 181–187.

[3] D. Choudhury, D., S. Nimbalkar, Seismic Passive Resistance by Pseudo-dynamic Method." Geotechnique, 55 (9) 2005, 699–702.
[4] D. Choudhury, K. S. Subba Rao, Seismic bearing capacity of shallow strip footings embedded in slope, Int. J. Geomech., 6(3) 2006, 176–184.
[5] L. Dormieux, A. Pecker, Seismic bearing capacity of foundations on cohesionless soil, J Geotech Eng, ASCE, 121(3) 1995, 300–303.
[6] P. Ghosh, Upper bound solutions of bearing capacity of strip footing by pseudo-dynamic approach, Acta Geotechnica, 3 2008, 115– 123.
[7] P. Ghosh, J. Kumar, Seismic bearing capacity of strip footings adjacent to slopes using the upper bound limit analysis, Electronic J. Geotech. Eng., 10 2005, 1–13.
[8] W. Hijab, A Note on the Centroid of a Logarithmic Spiral Sector, Geotechnique, 4(2) 1956, 96-99.
[9] J. Kumar, P. Ghosh, Seismic bearing capacity for embedded footings on sloping ground, Geotechnique, 56(2) 2006, 133–140.
[10] J. Kumar, N. Kumar, Seismic bearing capacity of rough footings on slopes using limit equilibrium, Geotechnique, 53(3), 2003, 363–369.
[11] A. Saha, A., S. Ghosh, Pseudo-dynamic Analysis for Bearing Capacity of Foundation Resting on c–Φ Soil, International Journal of Geotechnical Engineering, 9 (4) 2014, 379–387.
[12] S. Saran, V.K. Sud, S.C. Handa, Bearing capacity of footings adjacent to slopes, J. Geotech. Eng., 115(4) 1989, 553–573.
[13] S.K. Sarma, Y. C. Chen, Seismic bearing capacity of shallow strip footings near sloping round, Proc. of 5th SECED (Society for Earthquake and Civil Engineering Dynamics) Conf. European Seismic Design Practice, A. A. Balkema, Rotterdam, 1995, 505–512.
[14] S.K. Sarma, I. S. Iossifelis, Seismic bearing capacity factors of shallow strip footings, Geotechnique, 40(2) 1990, 265–273.
[15] A.H. Soubra, Seismic bearing capacity of shallow strip footings in seismic conditions, Proc Instn Civil Engrs Geotech Engr, 125(4) 1977, 230–241.
[16] A.H. Soubra, Upper bound solutions for bearing capacity of foundations, J Geotech Geoenviron Eng, ASCE, 125(1) 1999, 59–69.
[17] R.S. Steedman, X. Zeng, The influence of phase on the calculation of pseudo-static earth pressure on a retaining wall, Geotechnique, 40(1) 1990, 103–112, .